

Programmable Logic Devices in Experimental Quantum Optics

J. Stockton,* M. Armen, and H. Mabuchi

Norman Bridge Laboratory of Physics 12-33, California Institute of Technology, Pasadena, California 91125 USA

(Dated: October 25, 2018)

We discuss the unique capabilities of programmable logic devices (PLD's) for experimental quantum optics and describe basic procedures of design and implementation. Examples of advanced applications include optical metrology and feedback control of quantum dynamical systems. As a tutorial illustration of the PLD implementation process, a field programmable gate array (FPGA) controller is used to stabilize the output of a Fabry-Perot cavity.

I. INTRODUCTION

Automatic controllers are pervasive in experimental physics. Servos typically play a role behind the scenes, stabilizing environmental conditions (*e.g.* temperature, frequency and amplitude of driving lasers) for the physical system of primary interest (*e.g.* quantum dots, trapped atoms or molecules). But the system of interest can itself be the explicit object of sophisticated control strategies. An increasing number of experimental quantum systems are developing to the point where coherent dynamics occur at a time scale longer than that of available detectors and actuators [1, 2, 3]. This separation of time scales opens the door for real-time feedback control to be applied in quantum-mechanical scenarios.

New theoretical and experimental tools will be required to achieve quantum control objectives. Concerted efforts are currently being made to extend classical control theory to quantum problems where back-action cannot be ignored [5, 6]. Given the inherent nonlinearity of conditional quantum dynamics, optimal control laws cannot be practically implemented with analog circuits, necessitating fast digital control. Even for linear systems, programmable logic may be superior to analog methods when a precisely shaped transfer function is desired. For these reasons, one expects that programmable logic devices (PLD) with high processing speed and low latency will prove to be invaluable as quantum and classical controllers.

PLD's are already a standard tool in industry and some areas of science, but they have yet to attain widespread use in fields such as quantum optics and quantum information science. Our aim in this paper will be to convey a base level of knowledge required to use these devices in representative experimental setups. First, we motivate the use of programmable logic with some potential applications. We then describe the details of practical implementation, from determining the required hardware specifications to completing the design flow. Finally, we demonstrate this process with a familiar example of classical optical control by using a Field Programmable Gate Array (FPGA) to lock a Fabry-Perot cavity.

II. APPLICATIONS

An outstanding feature of PLD's is that they can implement complex non-linear logic with relatively low latency. Here 'latency' refers to the delay between the time that a signal is received as input and the time that a calculation based on it becomes available as output. This reaction time is of little consequence in many data-processing applications, but is critical in control loops. The control bandwidth of any servo is limited by the inverse of this delay.

In addition, most PLD's can be completely re-programmed in a matter of minutes, allowing for a high degree of design flexibility in experimental situations. Given a PLD with these capabilities, it is not difficult to imagine a variety of control applications related to quantum optics. Here we summarize a few potential examples, some of which are currently being developed.

A. Precise linear servos

In linear control tasks, PLD controllers have a distinct practical advantage over analog circuitry with regard to precision and flexibility. For example, it is a well known control problem to stabilize a plant over one of its resonances. An appropriate controller should precisely compensate the measured center frequency and quality factor of the resonance. When creating an analog servo the designer must work with discrete components (resistors, capacitors, etc.) whose impedances have a non-negligible error range. However a PLD transfer function can be specified digitally, making it much easier to closely match the system dynamics.

Figure 1 shows the near-compensation of a harmonic oscillator (HO) resonance with a PLD 'anti-harmonic-oscillator' (AHO) transfer function. (Actually, both transfer functions in the graph are implemented with a PLD by techniques described later.) Ideally, the HO transfer function will be transformed into an integrator transfer function (with a constant -90 degrees of phase) when multiplied by the AHO compensator. The deviation from a perfect integrator is due to a slight error in the assumed damping. Refinements to the AHO design could remove this non-ideality.

PLD's will obviously not replace every linear servo in

*Electronic address: jks@caltech.edu

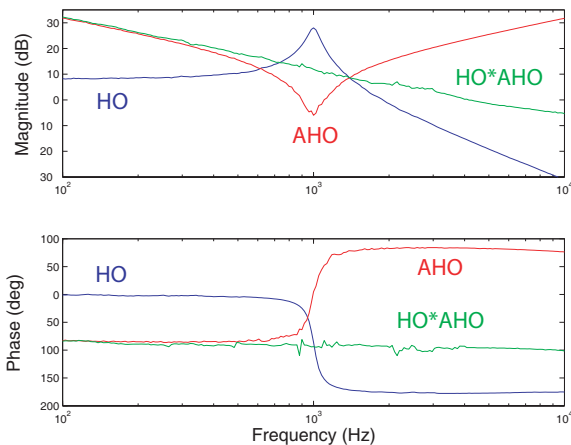


FIG. 1: The blue plot is a harmonic oscillator (HO) transfer function and the red plot is the anti-harmonic-oscillator (AHO) transfer function. The product of the two should resemble an integrator transfer function (green) with a constant -90 degree phase.

the typical laboratory, but the ability to optimize the stability of critical laser systems (for example) is a considerable resource. We detail the use of a PLD controller to optimally perform a linear control task in a later section.

B. Optimal measurement

In quantum feedback scenarios, either the measurement operators or the system Hamiltonian can be modulated in real time according to the information gained from a continuous measurement record.

Consider the case where only the measurement operators are adjusted. The goal of the entire measurement may be to most accurately determine the initial state of the system. Other situations may call for the measurement of only a single state parameter, where all other state variables are either assumed or neglected. The authors are currently developing a system of this type where the goal is to optimally measure the phase of a *single* pulse of light. We constrain ourselves to measuring pulses that are long enough to have their phase be well defined and also long enough to allow us to feedback the measurement signal multiple times before the pulse has been completely destroyed by the detectors.

Wiseman *et al.* have determined close-to-optimal measurement schemes for this system based on quantum trajectory theory [6]. In short, they consider the signal to be measured in an adaptive homodyne set-up where the pulse is mixed with a strong local oscillator whose phase, Φ , is continuously adjusted (within the duration of each pulse) according to the measured homodyne current, I . To first order, the job of the algorithm is to lock to the side of the interference fringe, thus Φ is adjusted until I is zero.

Despite this simplistic description, the general optimal algorithm ($f : I \Rightarrow \Phi$) is a highly non-linear function based on state estimation. It has been shown that the estimated state at any time is a function of only two parameters and the initial conditions. In terms of a scaled time v , the parameters are

$$A_v = \int_0^v I(u) e^{i\Phi(u)} du \quad (1)$$

$$B_v = - \int_0^v e^{2i\Phi(u)} du \quad (2)$$

The phase of the local oscillator is usually taken to be $\Phi(v) = \hat{\phi}(v) + \frac{\pi}{2}$ where $\hat{\phi}(v)$ is the phase estimate to be used during the course of feedback. If one were to stop the feedback at any time, the best phase estimate would be $\hat{\phi}_C(v) = \arg(C_v)$ where $C_v = A_v v + B_v A_v^*$. However, for subtle reasons, $\hat{\phi}_C(v)$ should not be used as the estimate during the course of the feedback.

One simple algorithm uses $\hat{\phi}(v) = \arg(A_v)$. With this choice, the algorithm simply reduces to a gain-scheduled integrator of the form

$$d\Phi(v) = \frac{I(v)}{\sqrt{v}} \quad (3)$$

where v is the time since the beginning of the pulse and the \sqrt{v} factor represents the effective gain. Currently, this algorithm is being implemented with an FPGA that creates the \sqrt{v} gain factor with a look-up table representation of the function as described in a later section.

More sophisticated algorithms (with optimal performance for certain squeezed states) have been proposed that use feedback of the form

$$\hat{\phi}(v) = \arg(C_v^{1-\epsilon(v)} A_v^{\epsilon(v)}) \quad (4)$$

where $\epsilon(v)$ is also a function of A_v and B_v . In this case, the algorithm is sufficiently complex that any analog implementation would be extremely difficult to design.

In any case, the non-linear, low latency behavior of PLD's suggest that they are a suitable tool for this task. Given that the form of a desired algorithm may change frequently with the introduction of realistic experimental complications, the rapid prototyping allowed by a PLD is also extremely convenient.

C. Feedback control

When the goal is control rather than optimal measurement, a non-trivial Hamiltonian of the system will be controlled by the measurement record. Consider the case of an atom drifting through the light field of a small Fabry-Perot cavity. As has been demonstrated, the position of the atom may be imprinted onto the output light of the cavity [3]. This information can potentially be mapped back onto the intensity and phase of the input laser with

the goal of trapping the atom in the cavity for extended periods of time [4].

Optimal control of the atom's position will require a complex predictor-corrector structure in the feedback loop at μsec time scales. If the associated calculations can be sufficiently reduced, a PLD with effective clocking speeds above a MHz will be able perform this task. Of course, the effectiveness of the control algorithm will depend on the assumed dynamics of the system from which it is derived. If the system needs to be described quantum mechanically, we should institute a conditional quantum state estimator. If a classical description is sufficient, we can use a less complicated algorithm. The performance of different controllers will be a strong indicator of the validity of our descriptions. The ability to quickly redesign the PLD will be particularly advantageous when exploring this boundary.

Hamiltonian feedback can also be used to manipulate the internal states of atomic and molecular systems. Numerous groups have become interested in shaping femtosecond laser pulses to drive transitions which may be inaccessible using traditional means [8]. This includes the ability to synthesize rare molecular compounds. For example, by iteratively reading the fluorescence spectrum of the system and intelligently moving in the parameter space of the pulse shape, one attempts to land at a shape conducive to creating the desired state or compound.

This procedure can happen in two regimes, 'learning control' or 'feedback control'. For learning control we consider using a new sample for every pulse, whereas for feedback control we consider using the same sample on every pulse. In the latter case, the algorithm assumes that the sample has a long enough dephasing time (memory) that a significant degree of coherence is retained between pulses. For either case, especially the second, a PLD based controller may have significant advantages over alternative controller architectures.

D. Decision and control for quantum information processing

In a generic quantum computing architecture, there exist classical logic steps which involve performing a coherent quantum operation conditioned on the result of a measurement. For example, quantum error correcting codes can combat decoherence by mapping measured errors to appropriate correction operators [7]. In an experiment, this measurement-operation procedure should be performed much faster than the dephasing rate of the system. If the operations can be performed quickly upon command, PLD's will be able to orchestrate these codes in a reliable and reconfigurable fashion with minimal delay.

Even for non-conditional algorithms, PLD's can streamline the implementation of complex instruction sets. In particular, groups working on ion trap computing have developed means of performing entangle-

ment algorithms [1], but with an extensive overhead of macroscopic equipment that requires detailed manual adjustment whenever the algorithm is changed. Without pushing its computational limits, a PLD can be made to streamline such logic networks. By using software defined algorithms, the users eliminate the time and risk of error associated with manual realignment of network components. Commercial magnetic resonance systems use PLD's for similar reasons.

As quantum computing architectures grow to the point where conditional and non-conditional algorithms must be integrated in a way that is fast and flexible, programmable logic will be able to handle the task in a convenient manner.

The success of any PLD controller will depend on its dynamic range and effective bandwidth. Next we discuss in more practical terms what levels of system performance can be reasonably expected from currently available PLD's.

III. DESIGN

A. Hardware

Once it is determined that a control algorithm needs to be implemented digitally, a designer is confronted with a wide array of possible controllers and corresponding acronyms. In addition to PLD's, the options include conventional microprocessor systems, DSP's (digital signal processors), and ASIC's (application specific integrated circuits). Of course, the choice of controller is highly dependent on the algorithm being implemented because each device has its own trade-offs. Microprocessor systems are general enough to allow for a simple means of programming complex algorithms. However, these systems rely on a single bus architecture which forms a significant bottleneck in signal processing applications. Overall throughput may be high, but a large delay limits typical controllers to slow applications with kHz scale bandwidths. In addition, unreliable operating systems may present undesirable interrupt signals during critical stages of processing. DSPs are specialized microprocessor systems with a multiple bus design that are optimized for signal processing applications. Due to their parallel architecture, DSP's can attain low-latency performance, but require a significant degree of high-level design expertise. ASIC's are like PLD's in that the user designs them from the gate level, but ASIC's are irreversibly hardwired with a single application. While PLD's generally have fewer resources available than ASIC's, they offer an efficient parallel computation structure along with reprogrammability and a relatively simple design process [9].

The market for PLD's is currently dominated by two companies: Xilinx and Altera. Devices from both companies have had extensive product development in industry, thus a substantial support network is available to designers. In choosing between PLD companies, several fac-

tors beyond the chip performance need to be considered, including the quality of the associated software environments. To obtain the maximum control bandwidth, we chose to work with a Field Programmable Gate Array (FPGA) from Xilinx.

The logic structure of a Xilinx FPGA is designed to handle arbitrary algorithm architectures. The FPGA mostly consists of a grid with thousands of Configurable Logic Blocks (CLB) connected by programmable interconnections. Each CLB contains a few small look-up tables which can serve as a simple logic elements (AND, OR, etc) when programmed. Also interspersed in this grid are larger blocks of RAM that can be programmed as user defined functions with a large domain and range. Since each logic element needs to be triggered to operate, the distribution of a uniform clock signal with constant frequency and phase is a considerable design issue. Thus FPGA architectures commonly have digital clock managers (DCM) or delay locked loops (DLL) that de-skew the clock signal across the device.

The performance of FPGA architectures has been impressively increasing in recent years. To give a current indication of their level of performance, we quote some of the characteristics of one of the top of the line devices available on the market today. The Xilinx Virtex II can contain up to 10 million system gates and have an internal clock frequency (f_C) up to 420 MHz. The input-output speed can be above 840 Mb/s which roughly matches the maximum speed of the best analog to digital converters (100 MSPS for a 12 bit sample Analog AD9432). This same FPGA has up to 192 SelectRAM blocks of 18 kbit each. Because a strong demand from industry drives the development of FPGA technology, these performance specifications will likely improve significantly in the short term future.

Of course these devices must be coupled to a board, introducing other practical issues. The system used in the cavity lock described below is a GVA-290 board (G.V. & Associates) with two Xilinx Virtex-E XCV1000E FPGA chips. Signals enter and exit the board through four input and four output SMA connectors. The signals are digitized by an ADC (Analog AD9432) at the input and converted back to analog by a DAC (Analog AD9762) at the output. Each ADC is located on a detachable daughter board, allowing for converter upgrades and the addition of customized components and filters. Both the ADCs and DACs have 12 bit resolution and are driven at the clock speed of 100 MHz. A crystal oscillator provides the clock signal to the FPGA, which distributes a synchronized signal internally with DLLs and also outputs the driving signal for the ADC and DAC at a controlled phase. Unlike standard models, the board was ordered with DC coupled inputs, allowing us to have broadband control to DC. Boards often come with anti-aliasing analog filters, but were not included here due to the substantial group delay a high-order filter can impose on the signal. The cost of this particular board including devices is approximately \$10,000, but it should be stressed

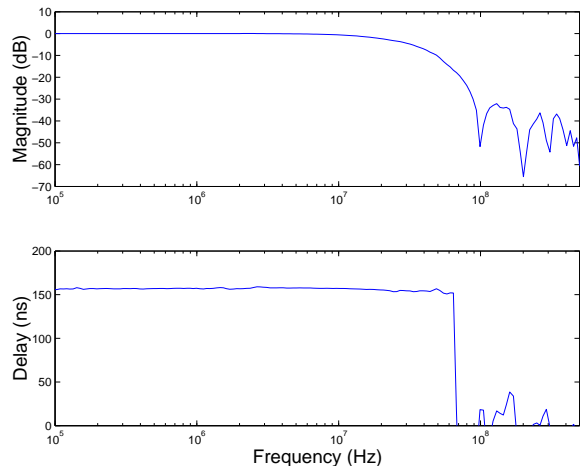


FIG. 2: The amplitude response and delay of the entire GV-290 board (ADC \rightarrow FPGA \rightarrow DAC). Notice that the delay below the Nyquist frequency ($f_C/2 = 50$ MHz) is ~ 160 ns. The phase response in the constant delay region is linear with slope proportional to the delay.

that functional systems could be assembled at far less cost.

Xilinx also offers a special academic program through which university researchers can obtain the necessary software environment and a limited range of hardware products.

We can now discuss the latency and throughput of our controller in more detail. The latency is defined as the amount of time for an algorithm to process a single sample all the way through. The throughput is defined as the number of samples (or bits) per second being output from the device. For example, consider a system of N components in series, each with the same sampling rate $f = \frac{1}{\tau}$. Also assume the system is ‘pipelined’ meaning that a new sample is loaded every τ seconds and samples are registered (values held) in-between components. In this case, the latency is $N\tau$, while the throughput is f . If this were a controller, the bandwidth of control would be limited to the inverse of the latency $\frac{1}{N\tau}$, not the throughput.

One of the principle advantages of FPGA technology is that the delay can be quite small. Consider the case where the FPGA of the GVA-290 board is programmed to pass a signal through without any manipulation. Figure 2 shows the transfer function and delay of this configuration. The ADC, FPGA, and DAC are all clocked at 100 MHz and each one takes a certain number of cycles (10 ns/cycle) to perform its function. The ADC imposes a delay of 10 cycles, the buffers of the FPGA impose a delay of 4 cycles, and the DAC only delays the signal about 1 cycle. Adding all this to a small delay from other components, we find that below the Nyquist frequency ($f_C/2 = 50$ MHz) the signal passes through at unity gain with a constant overall delay of ~ 160 ns. Thus the maximum control bandwidth for this device is

~ 6 MHz, and bandwidths in the tens of MHz may be anticipated with newer versions. If the FPGA algorithm is simple enough that the ADC dominates the delay, it may be desirable to use Flash ADCs that have less latency at the expense of a larger power consumption and smaller number of output bits.

If the FPGA performs a complex calculation that requires multiple logical steps in series, the delay is increased by an integer number of cycles and the effective bandwidth suffers. A typical example is that of the FIR filter mentioned below where, for B_U input bits, the sampling rate becomes f_C/B_U . For any general algorithm, care should be taken to minimize the number of serial elements before implementation. If possible, calculations should be performed in parallel and look-up tables should be used to evaluate complicated functions.

B. Software

The design process for a particular algorithm has been largely automated with implementation software environments like Foundation ISE (Xilinx). Once the design is entered via one of the options described below, the program steps through a series of compilation tasks before downloading onto the device. In order, the design is analyzed for syntactic errors, synthesized into a generic circuit, and implemented into an optimal bit stream appropriate to the particular device and board. The bit stream is then downloaded onto the device to achieve a stand-alone realization of the desired algorithm. Simulation programs are available at intermediate stages for debugging purposes. The latest version of Foundation ISE (4.1) compiles up to 100,000 gates/min. For reasonable designs, an entire design flow can be expected to take about 10 minutes. This allows for a rapid prototyping cycle which is one of the most desirable features of this technology.

Numerous algorithm entry options are available. Using a library of primitive components, one can create a schematic of the desired circuit. Abstract finite state machine diagrams can also be interpreted. The third option is a text based design written in either Verilog or VHDL (VHSIC Hardware Design Language).

As is common in technology standards, the choice of Verilog vs. VHDL has become a religious one for everyday practitioners. It is worth pointing out some of the accepted differences between the languages. Verilog is generally regarded as being easier to learn. A strong majority of engineers implementing commercial systems use Verilog. Historically, VHDL was meant as a description language before being adopted as a means of synthesis. As a result, VHDL is a much more strongly ‘typed’ language. The range of abstraction is also different between the two languages. Although there is a considerable overlap, Verilog extends to a lower level of abstraction while VHDL extends to a slightly higher level. For non-critical reasons, we chose to design in VHDL, hence we will dis-

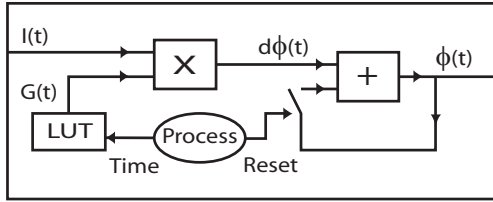
cuss the following designs in those terms. However, the discussion is abstract enough that most concepts apply to both languages.

To first order, VHDL is a text based description of a schematic design. The mapping between input and output bus variables consists of a series of abstractly defined components where output ports are connected to input ports with defined signal variables. Each component has an associated ‘entity’ and ‘architecture’, where an architecture is an instantiation of an entity. For example, a component with entity ‘op-amp’ (with only input and output ports defined) could have its functionality determined by the particular architecture ‘op27’. The internal workings of a particular architecture are can be specified in another VHDL file with more components that are defined elsewhere. In this way, the code lends itself nicely to nested level of detail and organized project design. Also one can easily swap out components by changing architectures, but not entities, within the code.

At some point in the hierarchy, primitive components must be called upon. The Xilinx software offers an extensive library of such components (AND, OR, etc.) for use with each particular device. In addition to these basic primitives, one can also create more complicated, but commonly used, components with the Xilinx ‘Core Generator’. These objects (adders, multipliers, filters, DSP elements) can be customized with user specified parameters.

Each component loads inputs and returns outputs triggered by an input clock signal. Hence, when designing in VHDL one thinks in terms of circuit diagrams where, on every clock cycle, events happen concurrently across the device. On the other hand, in traditional C-like computer languages events progress in a serial manner. At times, serial logic is convenient and in fact VHDL offers a restricted form of serial logic in a form known as a ‘process’. These processes are bits of C-like code that execute when triggered. Inside a process, variables can be manipulated with functions defined in other VHDL files. However, a signal can only be changed once within a process. For this and other reasons, processes are best used as referees to generate secondary triggering signals and logic. While processes can perform some level of math, the heavy lifting is best left to the components which have been streamlined for such purposes.

An appropriate use of a process is to initialize parameters and control timing. For example, Figure 3 demonstrates how the simple adaptive phase algorithm mentioned above is implemented. Both the VHDL and an equivalent schematic are shown. The photocurrent, I , enters the device and is multiplied by the time dependent gain factor, $G(t) = \frac{1}{\sqrt{t}}$, which is created by sending the time signal, t , through a look-up table (described below). The resulting signal, $d\Phi(t) = \frac{I(t)}{\sqrt{t}}$, is then sent to one port of an adder, with the other input port being wired to the output signal $\Phi(t)$. Because the output is connected to the input with a delay, the adder serves as an integrator and executes the relation $\Phi(t) = \Phi(t-1) + d\Phi(t)$ at every



VHDL Equivalent (the symbol -- precedes comments)

```

--first component is the look up table
--component format is 'instance: type'
--port map plugs signals into component ports; _# is label for bit size of bus

lut_num1 : ramblock_core
port map (EN=>vcc_sig, WE=>gnd_sig, RST=>gnd_sig, CLK=>clksys,
  ADDR=>time_8, DO=>Gtime_16, DI=>Gtime_16);

multiplier_num1 : multiplier_core
port map (A => I_12, B => Gtime_16, CLK => clksys, P => dphi_28);

--trim signal back down to size
dphi_12 <= dphi_28(27 downto 16);

adder_num1 : adder_core
port map (A => dphi_12, B => phi_21_a, Q => phi_21_b, CLK => clksys);

--plug signals together
phi_21_c <= phi_21_b;

--start process on clock change
PROCESS(clksys)
VARIABLE time : integer;
BEGIN
--trigger on rising edge of clock
IF clksys='1' AND clksys'EVENT THEN
IF time < tau_experiment THEN
phi_21_a <= phi_21_c;
phi_12 <= phi_21_c(20 downto 9);
ELSE
--zero signals during dead time
phi_21_a <= "0000000000000000000000";
phi_12 <= "00000000000000";
END IF;
IF time = tau_experiment+tau_dead THEN
time := 0;
END IF;
time := time+1;
--convert variable to signal
time_8 <= int_to_bus(time);
END IF;
END PROCESS;

```

FIG. 3: FPGA schematic and corresponding code for the adaptive phase measurement algorithm. In the schematic the process is not represented as a block component because it is coded in a serial manner.

time step. The ‘process’ plays an important role in this algorithm by initializing the integral value and creating the time signal. At the beginning of the pulse (integration), the process initializes t and Φ to zero. Every subsequent clock signal, the process increments t by one and lets the adder integrate up the signal. At the end of the pulse, the process waits for the next pulse then repeats the sequence. Figure 4 shows the algorithm in action. Through the integrator structure, Φ is adjusted until I is locked to zero. The overshoot is a result of the FPGA delay.

A single measurement using this algorithm is shown in Figure 4. Here the ‘pulse’ is a 50 μsec long time slice of a weak cw coherent beam. The feedback algorithm is sampling at 100 MHz with a delay less than 1 μsec . Because of the delay and other bandwidth limiting components in

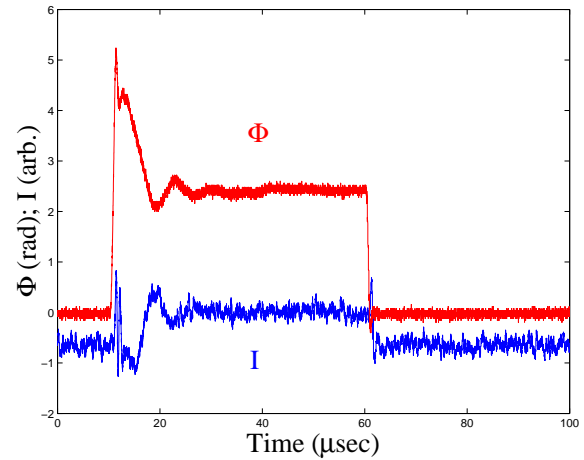


FIG. 4: The $\Phi(t)$ and $I(t)$ trajectories for the phase measurement of a single pulse of light. The current is locked to zero and the ending point of the phase is a rough estimate of the measured phase. The true phase measurement is a functional of both traces. The small oscillations are due to the delay in the loop.

the loop, our effective feedback bandwidth is limited to ~ 1 MHz.

As will be demonstrated below, Matlab plays a complementary role in the design process. It can be used to create the necessary coefficients and memory blocks used as parameters in the VHDL components. In particular, the Control and DSP toolboxes provide relevant functionality. Also, Simulink is a good tool for simulating the associated experiments, where delays and other realistic factors can complicate the dynamics. There exist software packages that attempt to directly translate from a Simulink design of an algorithm into equivalent VHDL, but these packages remain in early stages of development.

Due to their extensive utility, RAM look-up tables and filter components are worth discussing in greater detail.

1. Look-Up Tables

Most FPGA chips come equipped with large blocks of internal RAM that can be used as generalized functions or look-up tables (LUT). Given an amount of memory on a particular block, the user can decide on a certain number of input and output bits. During operation the RAM block returns the value held at the address specified by the input, effectively implementing the desired function. For example, on the XCV1000E, 160 blocks of $4096 = 2^{12}$ bits are available for internal use. (As noted above, the Virtex II devices have much larger 18 kbit blocks.) To make one block behave as the function f with B_i input bits, the designer would choose the output to be $B_o = 2^{12-B_i}$ bits. Possible partitions are $(B_i, B_o) \in [(1, 2048), (2, 1024), (3, 512), \dots, (8, 16), \dots, (12, 1)]$. Once a partition is chosen, the designer would use Matlab to define a block of data consisting of 2^{B_i} values each of

size B_o bits, and use this block of data as a parameter in the VHDL LUT component. If the discretization is a problem, more RAM blocks can be used to represent the function. If desired, the memory of a RAM block can also be dynamically written during operation. With this ability, an algorithm could easily adapt itself according to the signals it receives. Both the read and write operations (from/to one RAM address) only take a single clock cycle.

As mentioned above, these LUT functions play an extremely important role in speeding the functionality of non-linear algorithms. The application may be as simple as non-linear gain-scheduling of a controller or as complicated as full quantum-mechanical state estimation with the LUT performing functions based on assumed system parameters. In general, it is a matter of judgment how to partition complex algorithms, but any optimal partition will likely involve the use of these LUTs to perform the difficult parts of the calculation with minimal time delay.

2. Filters

PLD's have a clear edge over analog circuitry in non-linear processing, but they also have a potential advantage in implementing precise, generic linear filters and transfer functions.

A standard core element offered by Xilinx is the FIR (Finite Impulse Response) filter. The FIR is defined in discrete time as

$$y(n) = \sum_{i=0}^N a(i)u(n-i) \quad (5)$$

where $y(n)$ and $u(n)$ are the output and input at the discrete time n respectively. With standard Matlab functions (`firls`, `remez`) one can specify an arbitrary amplitude response and get out the corresponding $a(i)$ vector. The sampling frequency for a FIR element is $f_F = \frac{f_C}{B_U} = \frac{1}{\tau_F}$ where B_U is the number of bits chosen to represent $u(n)$. Of course, the filter is useless at shaping the response above this frequency. The group delay of the signal through the filter is approximately $\tau_F \frac{N}{2}$.

The range of attenuation is also a concern in the design of any filter. For an FPGA with B_F bits entering and leaving, the dynamic range is $20 \log(2^{B_F})$ dB. For our board with 12 bit ADC/DAC inputs and outputs, this corresponds to 70 dB. The designer should also have a sense of the size of the input and output signals. If the input signal is too high, the FPGA will rail; if the input is too low, it will fail to rise above the smallest bit size. To avoid these types of problems, broadband gain elements can be used at the input and output of the FPGA board.

A drawback of the FIR design is that it cannot be used to control the phase response of its transfer function. On the other hand, a generic continuous time linear transfer

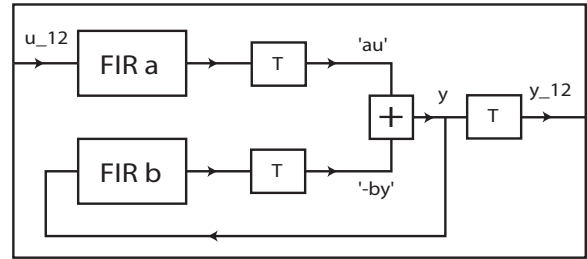


FIG. 5: Implementation of IIR filter. ‘T’ components trim a certain number of least significant bits from the data bus.

function

$$G_C(s) = \frac{c(N)s^N + c(N-1)s^{N-1} + \dots + c(1)}{d(N)s^N + d(N-1)s^{N-1} + \dots + d(1)} \quad (6)$$

where $Y_C = G_C U_C$, has phase control built in through the denominator. To approximate this function on a PLD, an Infinite Impulse Response (IIR) filter needs to be used.

One possible IIR design process illustrates this need. To generate a digital IIR design, first create $G_C(s)$ using standard control techniques (Nyquist, LQR, etc.). Next, convert from a continuous to a discrete transfer function

$$G_C \Rightarrow G_D(z) = \frac{a(0) + a(1)z^{-1} + \dots + a(N)z^{-N}}{b(0) + b(1)z^{-1} + \dots + b(N)z^{-N}} \quad (7)$$

with the Matlab function `c2d`. We have used the definition $Y_D = G_D U_D$ in the discrete time representation. Apply a z-transform ($z^{-1} \Rightarrow$ unit delay) to create the discrete time difference equation

$$y(n) = \sum_{i=0}^N a(i)u(n-i) - \sum_{i=1}^N b(i)y(n-i) \quad (8)$$

with the definition $b(0) = 1$. Finally, implement the difference equation in hardware as in Figure 5 with 2 FIR blocks and 1 adder.

With $b(n > 0) = 0$ the filter is just a FIR filter, however with $b(n > 0) \neq 0$ the output is fed back to itself. Hence an impulse response will have an infinite effect on the output. Of course, with internal feedback loops, the system is potentially unstable to noise and rounding errors. For this reason, among others, the Xilinx ‘Core Generator’ does not create flexible IIR modules.

However, with careful consideration of the number of bits required at each stage, a stable IIR filter can be created as in Figure 5. The sampling frequency for this simple architecture is $\frac{f_C}{2B_Y}$ where B_Y is the number of bits used to keep track of $y(n)$ internally. The factor of 2 results from the delay of both the adder and the FIR element. Because of the feedback, the IIR filter can achieve a given amplitude response with lower number of coefficients than the FIR filter. This means the filter delays the signal less. Even though the IIR has fewer

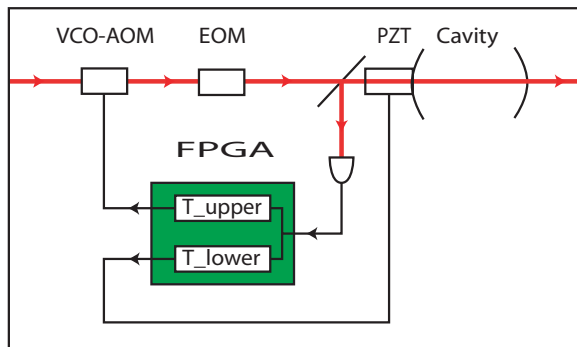


FIG. 6: Feedback architecture for a Fabry-Perot Cavity. The EOM puts sidebands on the beam necessary to generate the locking signal. The FPGA algorithm T_{upper} maps the error signal to the fast VCO-AOM frequency shifting combination. The FPGA algorithm T_{lower} maps the signal to the slow PZT.

coefficients than an analogous FIR filter, the coefficients of the IIR filter have to be specified to a greater degree of precision to achieve the same amplitude response.

IV. SPECIFIC EXAMPLE: CAVITY LOCK

We now discuss the use of an FPGA to perform a classical task necessary for low-noise experiments. High precision optical measurements demand laser intensity noise be minimized as much as possible. In the adaptive phase experiment mentioned above, the input laser is a Light-wave Nd:YAG model 126 (1064 nm) with an inherent broad relaxation oscillation noise peak at ~ 100 kHz. To perform broadband detection and control near 1 MHz, this intensity noise must be removed from the beam with a Fabry-Perot cavity.

A block diagram of the system is shown in Figure 6. The output intensity of the cavity is stabilized with the standard Pound-Drever-Hall method so that the error signal is created from a reflected carrier beam with sidebands. At low frequencies (below 100 Hz) the feedback loop is dominated by a piezoelectric element (PZT) which controls the length of the cavity. At higher frequencies and through the closing point of the servo, the feedback is from an AOM (Acousto-Optic Modulator) driven by a VCO (Voltage Controlled Oscillator) which adjusts the frequency of the input beam.

Given the control architecture of Figure 6, the design process can be made very systematic with the flexibility of the FPGA. Because the critical behavior of the servo will be dominated by the VCO-AOM loop, we concentrate on the design of T_U (T_{upper}). First, the transfer functions of the elements in the loop are measured. Here we find that the VCO-AOM combination behaves like a low-pass filter (T_V) with a corner at 100 kHz. The cavity itself can be modelled as a low-pass filter (T_C) with a corner at about 10 kHz (the cavity linewidth). The goal is

to design T_U such that the closed loop transfer function $T_{CL} = \frac{T_C T_V}{1 + T_C T_V T_U}$ is stable.

At this point, we can use the Matlab Control Toolbox to design an optimal T_U . One option is to provide the function `lqr` with the state space representations of T_V and T_C and an appropriate cost function to create the optimal T_U . The result simply tells us to make the combination $T_C T_V T_U$ behave like an integrator ($T_I = \frac{1}{s} = \frac{1}{j\omega}$) such that the controller satisfies the Nyquist criterion with 90 degrees of phase margin.

There are practical problems with this approach. In particular, the gain of T_U must be infinite for very low and very high frequencies. To remedy this, we flatten the response of T_U below 100 Hz (where the PZT arm takes over) and roll off the response at 300 kHz, beyond the closing point of the servo. So instead of making $T_U = \frac{T_L}{T_C T_V}$ we use $T_U = \frac{T_{LP1} T_{LP2}^2}{T_C T_V}$ where T_{LP1} is a low-pass filter with the corner at 100 Hz and T_{LP2} is a low-pass filter with the corner at 300 kHz.

To get high gain at frequencies below 100 Hz, we make T_L (T_{lower}) behave as a low-pass filter with a corner at only a few Hz. A better choice would be to implement T_L as a high-gain analog integrator, but we use the FPGA to implement T_L here for demonstration purposes.

Next, we generate proper IIR coefficients for both paths by the method described previously, treating T_L and T_U as the continuous transfer function G_C . With a clock frequency of 100 MHz and an internal sample size of $B_Y = 32$ bits, the IIR structure had an effective bandwidth of 1.5 MHz ($\frac{f_C}{2B_Y}$), which is adequate to generate the critical features of the transfer function.

Figures 7 and 8 show the desired and actual transfer functions of both arms. Each arm fails to match the desired phase and amplitude response in a similar way. First, because of the finite size of the sampling time, the actual phase response differs from the desired response as the frequency approaches the effective sampling frequency. In fact, this mismatch happens lower than the sampling frequency because of the delay of the IIR filter. Second, at low frequencies, the FPGA gives less gain than the desired result. This is due to the fact that we are dealing with finite precision coefficients. The price paid for having a large sampling frequency with small delay is that we have less control over the size of the low frequency gain. Finally, note that the PZT arm integrator achieves the full 70dB of expected range (input/output size is 12 bits).

The closed loop transfer function behavior for both arms matches our expectations for noise rejection at low frequencies. A mismatch at higher frequencies is due to inadequate modelling of the PZT and other components. (The PZT behaves more like a collection of oscillators with different resonances than a low pass filter.) Qualitatively, the FPGA lock was much more robust to high frequency noise than an analog version of the servo. This was likely due to the precise match to the plant dynamics near the unity gain point of the servo, achieved by the use of large FIR coefficients. However, the FPGA

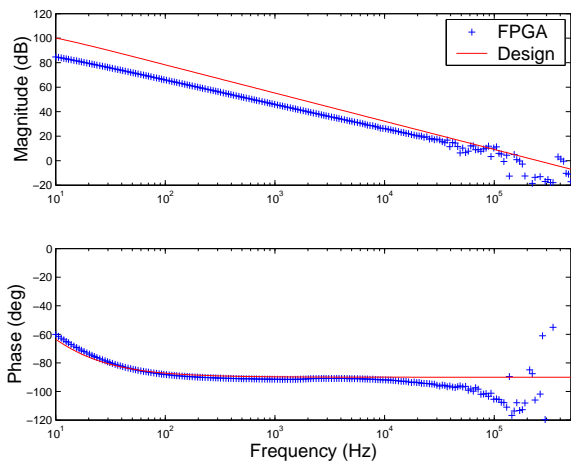


FIG. 7: Bode plot of T_{lower} (transfer function leading to PZT). The design is a low-pass filter which dominates control below ~ 100 Hz.

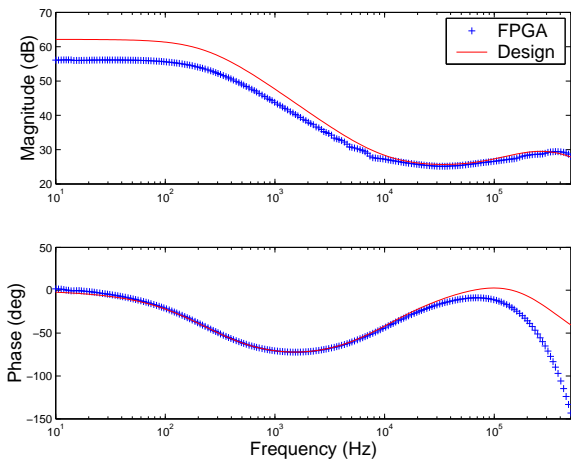


FIG. 8: Bode plot of T_{upper} (transfer function leading to VCO-AOM). The peak in phase is designed to stabilize the plant through the unity gain point.

lock was unable to retain the lock over time scales more than a few hours due to the saturated gain at very low

frequencies. This problem could easily be remedied by using an analog integrator with more DC gain to replace the FPGA PZT transfer function. The main advantage of the FPGA is its fast accurate response and, besides the demonstration presented here, there is no practical reason to use the FPGA for high-gain, low-frequency applications.

Finally, another feature of FPGA control is the possibility of adding logical automation to this system. Specifically, if the controller loses the lock, then the FPGA could be programmed to sense this condition, sweep for a signal, hone in, and re-acquire the lock. The abstract logical nature of VHDL code makes this task simple relative to the procedure needed to create an acquisition system using standard electronics.

V. SUMMARY

To demonstrate the use of programmable logic technology in an otherwise familiar setting, we have concentrated on a linear control application. We have used this example to convey the issues associated with a digital controller, including design, latency, and discretization. However, we have only hinted at the more interesting advanced applications in experimental quantum optics which are sure to develop more quickly because of this technology. FPGAs and similar devices are particularly suited to any physical system where non-linear mappings are desired between output and input variables within the natural dynamical time-scale. With these devices and sufficiently protected quantum systems in hand, the field of coherent quantum control may soon have enough speed to match the intelligence of its proposed controllers.

ACKNOWLEDGEMENTS

J.S. acknowledges the support of a Hertz Foundation Fellowship, and H.M. acknowledges the support of an A. P. Sloan Research Fellowship. This work was supported by the NSF under grant PHY-9987541, and by the ONR under Young Investigator Award N00014-00-1-0479.

-
- [1] C.A. Sackett et al., *Nature* **404**, 256 (2000).
 - [2] M. R. Andrews et al., *Science* **273**, 84 (1996).
 - [3] C. J. Hood et al., *Science* **287**, 1447 (2000).
 - [4] S. Habib, K. Jacobs, and H. Mabuchi, *Feedback control of atomic motion in an optical cavity*, Unpublished.
 - [5] A. C. Doherty et al., *Phys. Rev. A* **62**, 012105 (2000);
A. C. Doherty et al., *Phys. Rev. A* **63**, 062306 (2001).
 - [6] H. M. Wiseman and R. B. Killip, *Phys. Rev. A* **57**, 2169 (1998);
 - D. W. Berry and H. M. Wiseman, *Phys. Rev. A* **63**, 013813 (2000).
 - [7] M. A. Nielsen and I. L. Chuang, *Quantum Computation and Quantum Information* (Cambridge University Press, 2000).
 - [8] H. Rabitz et al., *Science* **288**, 824 (2000).
 - [9] D. Stranneby, *Digital Signal Processing* (Newnes, 2001).